Dyes and Pigments 121 (2015) 1–9

Contents lists available at ScienceDirect

Dyes and Pigments

journal homepage: www.elsevier.com/locate/dyepig

New acceptor–π-porphyrin–π-acceptor systems for solution-processed small molecule organic solar cells

Susana Arrechea [a], Agustín Molina-Ontoria [b], Ana Aljarilla [a], Pilar de la Cruz [a], Fernando Langa [a, *], Luis Echegoyen [b, *]

[a] Universidad de Castilla-La Mancha, Institute of Nanoscience, Nanotechnology and Molecular Materials (INAMOL), Campus de la Fábrica de Armas, Toledo, Spain
[b] Department of Chemistry, University of Texas at El Paso, El Paso, TX 79968, USA

ARTICLE INFO

Article history:
Received 23 March 2015
Received in revised form
23 April 2015
Accepted 27 April 2015
Available online 8 May 2015

Keywords:
Photovoltaics
Bulk heterojunction solar cells
Small molecule
Porphyrin
Thienylenevinylene
PCBM

ABSTRACT

Two new conjugated acceptor–donor–acceptor (A–π-D–π-A) compounds having a Zn-porphyrin acting as donor and linked by ethynylenes to one or two units of thienylenevinylene and capped by dicyanovinylene groups as acceptor units have been synthesized and their photophysical and electrochemical properties were investigated. These compounds were used as donor materials and $PC_{61}BM$ and $PC_{71}BM$ were used as acceptors in solution-processed bulk-heterojunction (BHJ) organic solar cells and the best photoconversion efficiency (PCE) obtained was 3.21%.

1. Introduction

Efficient production of clean and sustainable energy is one of the most important scientific challenges that the world faces today. Sunlight is the most abundant and one of the cleanest sources of energy, thus the efficient utilization of solar energy to prepare solar cells has attracted much attention from the scientific community [1–3]. The development of efficient organic photovoltaic (OPV) solar cells has attracted considerable interest as potential alternative solar energy sources to silicon-based solar cells, because of their distinct advantages of solution processability, low-cost, flexibility and roll-to-toll production possibilities. The bulk heterojunction (BHJ) approach is the most efficient to date, which consists of a nanometer scale interpenetrating network of an electron-accepting, typically fullerene, phase and a light-harvesting electron-donor phase, such as a polymer or a small molecule. Polymer solar cells (PSCs) underwent significant progress in the past decades, thanks to the judicious design of narrow band-gap copolymers, optimization of the nanoscale morphologies of the photoactive layers and enhanced carriers mobilities, which have led to power conversion efficiencies (PCEs) of 10% for single-junction PSCs [4,5] and up to 11% for tandem PSCs [6]. Nonetheless, there are issues with the synthesis of conjugated polymers for photovoltaic applications, such as difficult purification, poor batch-to-batch reproducibility and so on.

Solution processed small-molecule organic solar cells (SMBHJ), are an emerging alternative to the polymer counterparts, and these have rapidly developed in recent years, which offer potential advantages, such as better defined structures, easier purification and better reproducibility [6–9]. Thus far, power conversion efficiencies exceeding 9% have been reported for solution-processed small molecule single junction devices [10–15].

Inspired by natural photosynthetic organisms, where chlorophylls absorb light for energy conversion, and because of intense Soret band at around 400 nm and the Q bands close to 600 nm, porphyrins and their derivatives are excellent building blocks for the construction of light harvesting architectures [16]. Porphyrins are among the best sensitizers in Dye Sensitized Solar cells (DSSCs) [17–22] showing performances as high as 12% [23]. However, the utilization of porphyrins as active materials in solution-processed BHJ solar cells has been limited [24–33] despite their natural tendency to form aggregates by π–π stacking interactions [34].

In this article we report the synthesis of two new conjugated acceptor–donor–acceptor (A–π-D–π-A) molecules **1a** and **1b**

* Corresponding authors.
E-mail address: Fernando.Langa@uclm.es (F. Langa).

http://dx.doi.org/10.1016/j.dyepig.2015.04.037
0143-7208/

(Fig. 1), along with their photophysical and electrochemical properties, as well as their performance in solution-processed SMBHJ. Both compounds were used as the p type layer with the Zn-porphyrin core acting as a donor linked by ethynylenes to one or two units of thienylenevinylene and capped by dicyanovinylene groups as acceptor units. Ethynylenes were chosen to make the systems planar and hexyl chains were attached on the thiophene units to enhance their solubility. $PC_{61}BM$ and $PC_{71}BM$ were used as acceptor components in the devices.

2. Experimental section

2.1. Experimental details

Experimental details are given in the Supporting information.

2.2. Synthetic procedures

2.2.1. General synthetic procedure for *3a*, *b* [35]

To a solution of **5a**, **b** [36] (1 eq) in carbon tetrachloride (CCl_4, 1.25 mL/mmol) was added $PhI(OCOCF_3)_2$ (0.55 eq) and molecular iodine (I_2, 0.5 eq). The mixture was stirred at room temperature. The reaction was quenched with a saturated solution of sodium thiosulfate (Na_2SO_3 sat.) while stirring for 15 min and extracted with CH_2Cl_2. The combined organic phases were dried over anhydrous $MgSO_4$ and filtered. The solvent was removed by rotary evaporation.

2.2.2. 5-Iodo-3,4-dihexyl-2-thiophencarboxaldehyde (*3a*)

Using the general procedure previously described, **5a** (1.8 mmol, 500 mg) was reacted with $PhI(OCOCF_3)_2$ (1.0 mmol, 416 mg) and I_2 (0.9 mmol, 226 mg) in 2.2 mL of CCl_4. The product was purified by column chromatography (silica gel, hexane–$CHCl_3$, 7:3). **3a** was obtained as a yellow oil (610 mg, 1.51 mmol, 84% yield). ^{1}H NMR (400 MHz, $CDCl_3$) δ/ppm: 9.90 (s, 1H), 2.94–2.90 (m, 2H), 2.57–2.53 (m, 2H), 1.64–1.57 (m, 4H), 1.39–1.31 (m, 12H), 0.93–0.88 (m, 6H). ^{13}C NMR (100 MHz, $CDCl_3$) δ/ppm: 181.2, 150.5, 148.4, 143.0, 89.7, 32.3, 31.5, 31.4, 30.6, 29.7, 29.3, 29.3, 27.8, 22.6, 22.5, 14.1, 14.0. MALDI-TOF MS (*m*/*z*): $[M]^+$ calculated for $C_{17}H_{27}IOS$: 406.08; found: 406.08. FT-IR (ATR) υ/cm^{-1}: 2923, 2854, 1654, 1523, 1461, 1427, 1365, 1222, 1126, 1079, 721, 674.

2.2.3. (E)-1-(5-formyl-3,4-dihexyl-2-thienyl)-2-(5-iodo-3′,4′-dihexyl-2′-thienyl)ethylene (*3b*)

Using the general procedure previously described, **5b** (0.6 mmol, 338 mg) was reacted with $PhI(OCOCF_3)_2$ (0.3 mmol, 142 mg), I_2 (0.3 mmol, 77 mg) in 0.75 mL of CCl_4. The product was purified by column chromatography (silica gel, hexane–$CHCl_3$, 3:2). **3b** was obtained as a yellow oil (255 mg, 0.37 mmol, 62% yield). ^{1}H NMR (400 MHz, $CDCl_3$) δ/ppm: 9.98 (s, 1H), 7.19 (d, 1H, J = 15.5 Hz), 6.97 (d, 1H, J = 15.5 Hz), 2.84 (t, 2H, J = 7.7 Hz), 2.64 (t, 2H, J = 7.7 Hz), 2.58 (t, 2H, J = 7.7 Hz), 2.49 (t, 2H, J = 7.7 Hz), 1.50–1.27 (m, 32H), 0.94–0.88 (m, 12H). ^{13}C NMR (100 MHz, $CDCl_3$) δ/ppm: 181.9, 153.0, 147.7, 146.6, 141.8, 141.6, 141.0, 134.8, 123.1, 118.8, 75.5, 32.3, 31.6, 31.5, 31.4, 31.1, 31.0, 29.8, 29.3, 27.9, 27.1, 26.4, 22.6, 22.5, 14.1, 14.05. MALDI-TOF MS (*m*/*z*): $[M]^+$ calculated for $C_{35}H_{55}IOS_2$: 682.27; found: 683.49. FT-IR (ATR) υ/cm^{-1}: 2923, 2850, 1654, 1600, 1523, 1461, 1403, 1375, 1249, 1211, 933, 725, 678, 663.

2.2.4. Synthesis of 5,15-dimesitylporphyrin [37]

A solution of corresponding dipyrromethane [38] (14.4 mmol, 2.10 g) and 2,4,6-trimethylbenzaldehyde (14.4 mmol, 2.1 mL) in 1.40 L of $CHCl_3$ was treated with $BF_3O(C_2H_5)_2$ (4.7 mmol, 0.6 mL). The mixture was stirred for 3 h. DDQ (21.5 mmol, 4.9 g) was added and the reaction mixture was stirred for 1 h. Et_3N (2.0 mL) was added and stirred during 30 min. The solvent was removed by rotary evaporation and the solid was purified by column chromatography (silica gel, hexane–$CHCl_3$, 1:1). 5,15-Dimesitylporphyrin was obtained as a purple solid (1400 mg, 2.56 mmol, 35% yield). ^{1}H NMR (400 MHz, $CDCl_3$) δ/ppm: 10.25 (s, 2H), 9.35 (d, 4H, J = 4.5 Hz), 8.91 (d, 4H, J = 4.5 Hz), 7.35 (s, 4H), 2.69 (s, 6H), 1.87 (s, 12H), −3.04 (s, 2H). ^{13}C NMR (100 MHz, $CDCl_3$) δ/ppm: 146.8, 145.4, 139.5, 137.8, 137.6, 131.8, 130.0, 127.8, 117.3, 104.6, 21.7, 21.5. MALDI-TOF MS (*m*/*z*): $[M]^+$ calculated for $C_{38}H_{34}N_4$: 546.09; found: 546.28. FT-IR (ATR) υ/cm^{-1}: 3305, 1828, 1604, 1411, 1373, 1319, 1234, 1052, 950, 852, 782, 736, 694, 617.

2.2.5. Synthesis of [5,15-dimesitylporphyrinato] zinc (II) [39]

To a solution of 5,15-dimesitylporphyrin (2.5 mmol, 1.35 g) in 209 mL of $CHCl_3$, was added a solution of $Zn(OAc)_2 \cdot 2H_2O$ (12.3 mmol, 2.26 g) in 6.2 mL of MeOH. The mixture was stirred 18 h. The reaction was quenched with water and extracted with $CHCl_3$ (3 × 100 mL). The combined organic extract was dried over anhydrous $MgSO_4$ and filtered. The solvent was removed by rotary evaporation. The product was purified by column chromatography (silica gel, hexane–$CHCl_3$, 1:1). The product [5,15-dimesitylporphyrinato] zinc (II), was obtained as a purple solid (1.51 g, 2.47 mmol, 99% yield). ^{1}H NMR (400 MHz, $CDCl_3$) δ/ppm: 10.27 (s, 2H), 9.41 (d, 4H, J = 4.4 Hz), 9.00 (d, 4H, J = 4.4 Hz), 7.35 (s, 4H), 2.69 (s, 6H), 1.85 (s, 12H). ^{13}C NMR (100 MHz, $CDCl_3$) δ/ppm: 149.8, 149.4, 139.3, 138.8, 135.7, 132.1, 131.3, 127.7, 118.2, 105.5, 21.7, 21.5. MALDI-TOF MS (*m*/*z*): $[M]^+$ calculate for $C_{38}H_{32}N_4Zn$: 608.57; found: 608.19. FT-IR (ATR) υ/cm^{-1}: 1816, 1608, 1438, 1388, 1318, 1211, 1052, 856, 786, 728, 701, 617.

2.2.6. Synthesis of [5,15-dibromo-10,20-dimesitylporphyrinato] zinc (II)

To a solution of [5,15-dimesitylporphyrinato] zinc (II) (1.5 mmol, 920 mg) in 80 mL of $CHCl_3$, *N*-bromosuccinimide (NBS) (3.0 mmol, 536 mg) and 1 mL of pyridine were added. The mixture was stirred

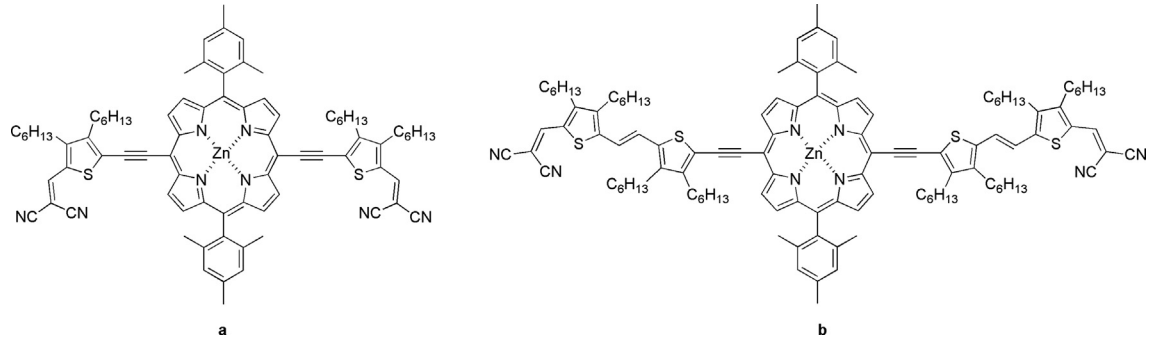

Fig. 1. Structures of **1a** and **1b**.

30 min and quenched with acetone. The solvent was removed by rotary evaporation and the solid was purified by column chromatography (silica gel, hexane–$CHCl_3$, 7:3). The product [5,15-dibromo-10,20-dimesitylporphyrinato] zinc (II) was obtained as a purple solid (1.11 g, 1.45 mmol, 98% yield). ^{1}H NMR (400 MHz, $CDCl_3$) δ/ppm: 9.59 (d, 4H, J = 4.6 Hz), 8.71 (d, 4H, J = 4.6 Hz), 7.80 (s, 4H), 2.65 (s, 6H), 1.80 (s, 12H). ^{13}C NMR (100 MHz, $CDCl_3$) δ/ppm: 150.5, 149.9, 139.1, 138.8, 137.6, 133.3, 132.0, 127.7, 122.3, 120.1, 104.1, 55.4, 21.6, 21.4. MALDI-TOF MS (m/z): $[M]^+$ calculate for $C_{38}H_{30}Br_2N_4Zn$: 766.73; found: 766.01. FT-IR (ATR) υ/cm^{-1}: 1808, 1604, 1423, 1373, 1315, 1203, 1072, 995, 860, 786, 740, 694, 628, 609.

*2.2.7. Synthesis of [5,15-bis-(trimethylsilyl)ethynyl-10,20-dimesitylporphyrinato] zinc (II) (**2**)*

In a Schlenk tube under an argon atmosphere, a solution of [5,15-dibromo-10,20-dimesitylporphyrinato] zinc (II) (1.4 mmol, 1.10 g) in 62 mL of THF and 3 mL of Et_3N was added over a mixture of $Pd(PPh_3)_2Cl_2$ (0.1 mmol, 54 mg) and CuI (0.07 mmol, 13 mg). Afterwards, trimethylsilylacetylene (5.4 mmol, 0.8 mL) was added. The mixture was stirred 18 h. The solvent was removed by rotary evaporation and the solid was purified by column chromatography (silica gel, hexane–$CHCl_3$, 7:3) and recrystallized from CH_2Cl_2/MeOH. **2** was obtained as a purple solid (1.07 g, 1.35 mmol, 97% yield). ^{1}H NMR (400 MHz, $CDCl_3$) δ/ppm: 9.68 (d, 4H, J = 4.6 Hz), 8.79 (d, 4H, J = 4.6 Hz), 7.33 (s, 4H), 2.68 (s, 6H), 1.86 (s, 12H), 0.62 (s, 18H). ^{13}C NMR (100 MHz, $CDCl_3$) δ/ppm: 152.1, 149.9, 139.0, 138.4, 137.6, 131.9, 131.7, 131.4, 127.7, 120.9, 107.4, 101.5, 100.6, 21.5, 21.5, 0.3. MALDI-TOF MS (m/z): $[M]^+$ calculated for $C_{48}H_{48}N_4Si_2Zn$: 800.58; found: 800.27. FT-IR (ATR) υ/cm^{-1}: 2136, 1808, 1604, 1438, 1380, 1334, 1203, 1072, 995, 860, 786, 736, 694, 617.

2.2.8. Synthesis of [5,15-bis-(ethynyl)-10,20-dimesitylporphyrinato] zinc (II)

To a solution of **2** (0.7 mmol, 550 mg) in 150 mL of CH_2Cl_2, was added TBAF 1 M in THF (1.65 mmol, 1.65 mL). The solution was stirred at room temperature for 2 h and treated with $CaCl_2$ (8.2 mmol, 912 mg). The reaction was hydrolyzed with water and extracted with $CHCl_3$ (3 × 150 mL). The combined organic extract was dried over anhydrous $MgSO_4$ and filtered; finally, the solvent was removed by rotary evaporation. The deprotected product was quantitatively obtained and it was used in the next synthetic step without further purification.

2.2.8.1. General procedure for the Sonogashira coupling reactions. Under an argon atmosphere, a solution of [5,15-bis-(ethynyl)-10,20-dimesitylporphyrinato] zinc (II) (1 eq), the corresponding aldehyde (**3a**–**b**) (3 eq) and freshly distilled Et_3N (45 mL/mmol) in THF (230 mL/mmol) was added over a mixture of $Pd_2(dba)_3$ (0.6 eq) and $AsPh_3$ (3.8 eq). The reaction mixture was refluxed for 18 h. The solvent was removed by rotary evaporation and the solid was purified by column chromatography (silica gel, hexane–CH_2Cl_2, 7:3) followed by recrystallization from CH_2Cl_2/MeOH.

4a: Using the general procedure previously described, [5,15-bis-(ethynyl)-10,20-dimesitylporphyrinato] zinc (II) (0.34 mmol, 658 mg), **3a** (1.02 mmol, 417 mg), 15 mL of Et_3N in 79 mL of THF were allowed to react. **4a** was obtained as a green solid (337 mg, 0.22 mmol, 81% yield). ^{1}H NMR (400 MHz, $CDCl_3$) δ/ppm: 9.49 (d, 4H, J = 4.4 Hz), 9.16 (s, 2H), 8.75 (d, 4H, J = 4.4 Hz), 7.33 (s, 4H), 2.99 (t, 4H, J = 7.6 Hz), 2.80 (t, 4H, J = 7.6 Hz), 2.69 (s, 6H), 1.89 (s, 12H), 1.60 (t, 4H, J = 7.2 Hz), 1.54 (t, 4H, J = 7.2 Hz), 1.43–1.22 (m, 24H), 0.93 (t, 6H, J = 6.4 Hz), 0.77 (t, 6H, J = 7.0 Hz). ^{13}C NMR (100 MHz, $CDCl_3$) δ/ppm: 207.2, 181.2, 151.7, 151.6, 150.1, 148.2, 139.00, 138.1, 137.9, 137.3, 131.9, 131.2, 129.4, 127.8, 122.0, 103.1, 100.1, 89.5, 32.3, 31.8, 31.6, 30.9, 30.9, 29.7, 29.4, 28.7, 27.7, 22.7, 22.6, 21.6, 21.5, 14.1, 14.0. MALDI-TOF MS (m/z): $[M]^+$ calculated for $C_{76}H_{84}N_4O_2S_2Zn$: 1212.53; found: 1212.53. FT-IR (ATR) υ/cm^{-1}: 2919, 2854, 2175, 2053, 1650, 1612, 1489, 1438, 1403, 1330, 1284, 1207, 1150, 995, 937, 848, 790, 709.

4b: Using the general procedure previously described, [5,15-bis-(ethynyl)-10,20-dimesitylporphyrinato] zinc (II) (0.34 mmol, 658 mg), **3b** (1.02 mmol, 702 mg), 15 mL of Et_3N in 79 mL of THF were allowed to react. **4b** was obtained as a green solid (246 mg, 0.14, 71%). ^{1}H NMR (400 MHz, CDCl3) δ/ppm: 9.56 (s, 1H), 9.55 (d, 4H, J = 4.6 Hz), 8.73 (d, 4H, J = 4.6 Hz), 7.32 (s, 4H), 7.32 (d, 2H, J = 15.5 Hz), 7.08 (d, 2H, J = 15.5 Hz), 3.05 (t, 4H, J = 7.9 Hz), 2.79 (t, 4H, J = 7.9 Hz), 2.75 (t, 4H, J = 8.3 Hz), 2.68 (s, 6H), 2.66 (t, 4H, J = 7.2 Hz), 1.91 (t, 4H, J = 7.2 Hz), 1.89 (s, 12H), 1.67–1.31 (m, 60H), 1.00–0.91 (m, 18H), 0.80 (t, 6H, J = 7.2 Hz). ^{13}C NMR (100 MHz, CDCl3) δ/ppm: 181.7, 153.1, 151.6, 149.7, 148.5, 146.9, 142.7, 141.9, 139.0, 138.3, 137.7, 137.3, 134.6, 131.5, 131.1, 127.7, 132.5, 121.5, 119.0, 118.9, 101.2, 100.8, 90.7, 32.2, 31.8, 31.7, 31.6, 31.5, 31.2, 30.9, 29.7, 29.4, 29.3, 29.2, 29.1, 27.5, 27.1, 26.4, 22.7, 22.6, 21.5, 21.4, 14.2, 14.1, 14.0, 13.9. MALDI-TOF MS (m/z): $[M]^+$ calculated for $C_{112}H_{140}N_4O_2S_4Zn$: 1764.92; found: 1765.07. FT-IR (ATR) υ/cm^{-1}: 2919, 2854, 2175, 1646, 1592, 1500, 1454, 1388, 1338, 1292, 1207, 1095, 998, 929, 852, 790, 709.

2.2.8.2. General procedure for the Knoevenagel condensations. To a solution of **4a**, **b** (1 eq) in 25 mL/mmol of CH_2Cl_2, malononitrile (3 eq) and 3 drops of Et_3N were added. The reaction mixture was stirred for 18 h and quenched by the addition of water and extracted with $CHCl_3$ (3 × 150 mL). The combined organic extract was dried over anhydrous $MgSO_4$ and filtered. The solvent was removed by rotary evaporation. The product was purified by column chromatography (silica gel, hexane–CH_2Cl_2, 1:1) and recrystallized with CH_2Cl_2:MeOH.

1a: Using the general procedure previously described, **4a** (0.08 mmol, 100 mg) in 2 mL of CH_2Cl_2 were allowed to react with malononitrile (0.25 mmol, 16 mg). **1a** was obtained as a green solid (87 mg, 0.06 mmol, 81% yield). M. p. >300 °C. ^{1}H NMR (400 MHz, $CDCl_3$) δ/ppm: 9.16 (s, 4H), 8.75 (d, 4H, J = 4.2 Hz), 7.89 (s, 2H), 7.37 (s, 4H), 3.84 (m, 4H), 2.76 (m, 4H), 2.71 (s, 6H), 1.96 (s, 12H), 1.76 (m, 4H), 1.64–1.74 (m, 12H), 1.27–1.22 (m, 16H), 0.97 (m, 6H), 0.76 (t, 6H, J = 6.7 Hz). ^{13}C NMR (100 MHz, $CDCl_3$) δ/ppm: 154.3, 151.6, 150.3, 147.7, 147.4, 138.9, 138.1, 137.8, 132.2, 131.0, 130.8, 127.9, 122.8, 115.1, 113.9, 106.3, 99.5, 89.4, 75.2, 32.3, 31.7, 31.6, 31.5, 30.9, 30.7, 30.2, 29.7, 29.6, 29.1, 28.8, 22.6, 21.6, 21.5, 14.1, 14.0. MALDI-TOF MS (m/z): $[M]^+$ calculated for $C_{82}H_{84}N_8S_2Zn$: 1308.53; found: 1308.56. FT-IR (ATR) υ/cm^{-1}: 2923, 2854, 2225, 2154, 2053, 1612, 1489, 1465, 1403, 1330, 1288, 1249, 1203, 1083, 998, 937, 850, 790, 711.

1b: Using the general procedure previously described, **4b** (0.2 mmol, 295 mg) in 3 mL of CH_2Cl_2, malononitrile (0.5 mmol, 33 mg). **1b** was obtained as a green solid (246 mg, 0.06 mmol, 79% yield). M. p. > 300 °C. ^{1}H NMR (400 MHz, $CDCl_3$) δ/ppm: 9.46 (d, 4H, J = 4.4 Hz), 8.68 (d, 4H, J = 4.4 Hz), 7.69 (s, 2H), 7.28 (s, 4H), 7.21 (d, 2H, J = 15.6 Hz), 6.96 (d, 2H, J = 15.6 Hz), 2.96 (t, 4H, J = 7.7 Hz), 2.70 (t, 4H, J = 7.7 Hz), 2.62 (s, 6H), 2.57 (m, 8H), 1.85 (s, 12H), 1.60–1.54 (m, 8H), 1.49–1.26 (m, 56H), 0.94–0.56 (m, 18H), 0.73 (t, 6H, J = 7.0 Hz). ^{13}C NMR (100 MHz, $CDCl_3$) δ/ppm: 155.9, 151.6, 149.8, 149.1, 148.8, 147.2, 144.1, 141.6, 139.0, 138.2, 137.8, 137.2, 131.6, 131.1, 128.3, 127.8, 125.7, 120.1, 118.2, 115.6, 114.2, 101.4, 101.2, 90.8, 73.1, 32.2, 31.8, 31.6, 31.6, 31.5, 31.0, 31.9, 29.7, 29.5, 29.3, 29.2, 27.8, 27.5, 26.8, 22.8, 22.7, 22.6, 22.6. MALDI-TOF MS (m/z): $[M]^+$ calculated for $C_{118}H_{140}N_8S_4Zn$: 1860.94; found: 1861.94. FT-IR (ATR) υ/cm^{-1}: 2928, 2856, 2217, 2171, 1552, 1500, 1457, 1399, 1336, 1288, 1209, 1091, 998, 929, 854, 794, 711.

3. Results and discussion

3.1. Synthesis and characterizations

Scheme 1 illustrates the synthetic route used to obtain organic semiconductor compounds **1a** and **1b**, starting from *bis*-

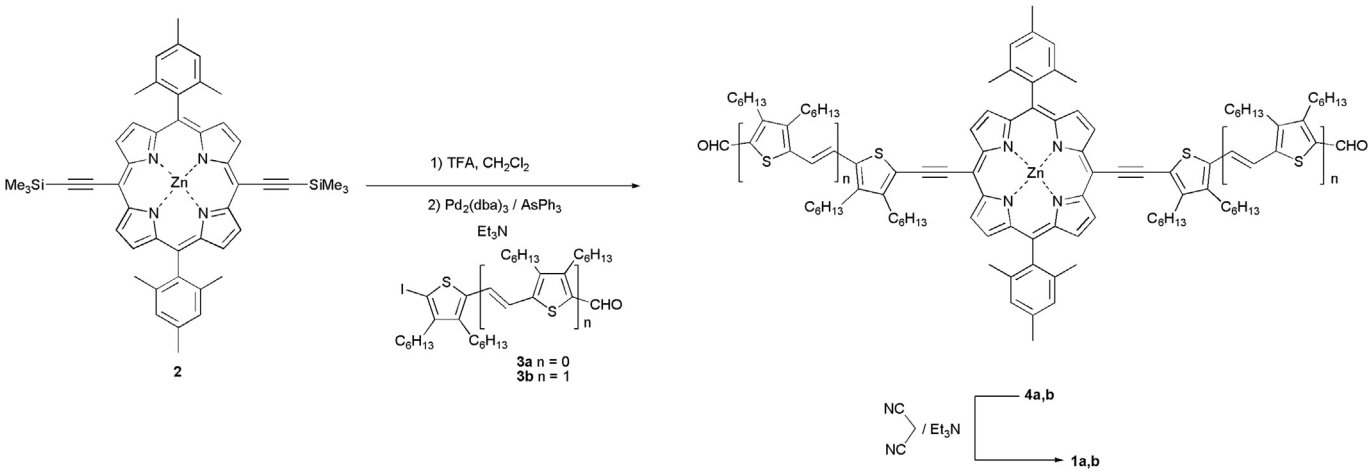

Scheme 1. Synthetic route to chromophores **1a** and **1b**.

trimethylsilyl porphyrin **2**. The trimethylsilyl group was quantitatively removed by hydrolysis with TBAF and, without further purification, reacted with the corresponding iodoaldehyde **3a**, **b** under Pd-catalyzed Sonogashira coupling conditions to afford the bisaldehydes **4a**, **b** in 81% and 71% yields, respectively. The ^{1}H NMR spectra of **4a**, **b** show the expected signals for both the porphyrin and the thienylenevinylene moieties and the aldehyde protons are observed at 9.16 ppm and 9.56 ppm, respectively. Compound **4b**, only showed the *trans* configuration of the double bond, which was confirmed by a coupling constant of 15.6 Hz. Finally, the target compounds **1a**, **b** were obtained by Knoevenagel condensations of **4a**, **b** with malononitrile in the presence of triethylamine in 81% and 79% yields, respectively. In the ^{1}H NMR spectra of **1a**, **b**, the aldehyde hydrogen signals are not observed and new vinylic hydrogens signals were observed at 7.89 ppm and 7.69 ppm, respectively, indicating the successful condensation. The mass spectrum of compounds **1a** showed the molecular ion peak at *m*/*z* 1308.56 amu, while that of compound **1b** exhibited the molecular ion peak at *m*/*z* 1861.94 amu.

Previously, iodoaldehydes **3a**, **b** were prepared by the reaction of the aldehydes **5a**, **b**, with molecular iodine (I_2), and bistrifluoroacetoxyiodobenzene ($PhI(OCOCF_3)_2$) in 84% and 62% yield according to Scheme 2 [35].

All compounds were satisfactorily characterized by ^{1}H and ^{13}C NMR, FT-IR and MALDI-MS spectrometry (see the Experimental section and the Supporting information for synthetic details and full analytical and spectroscopic characterizations).

The thermal stabilities of compounds **1a** and **1b** were evaluated by thermogravimetric analysis (TGA). Compounds **1a**, **b** display excellent thermal stabilities up to 300 °C with Td of 369 °C and 374 °C for **1a** and **1b**, respectively (Fig. S29), which are appropriate for photovoltaic applications.

3.2. Optical properties

The optical properties of **1a** and **1b** in CH_2Cl_2 solutions as well as of their thin-films are shown in Fig. 1 and the characteristics of semiconductors **1a** and **1b** are collected in Table 1. The UV–Vis absorption spectra of the precursor aldehydes (**4a**, **b**) and of the final compounds **1a**, **b** in solution exhibit a panchromatic absorption in the visible region. These spectra show the Soret band (λ_{max} = 465 nm and 499 nm respectively) bathochromically shifted, with respect to the Soret band in the precursor porphyrin **2** (λ_{max} = 435 nm, Fig. S30). New intense broad bands are observed (at λ_{max} = 668 nm for **4a** and 698 nm for **4b**), assigned to intramolecular charge transfer (ICT) (Fig. S30). In solution, **1a** and **1b** show absorption ranges from 400 nm to 750 nm with a valley centered at 600 nm. The introduction of the malononitrile fragments (**1a**, **b**) lead to a bathochromic shift of both bands (λ_{max} = 499 and 698 for **1a** and 497 and 705 nm for **1b**) with respect to the corresponding aldehydes (**4a**, **b**) as a consequence of the extension of the conjugation and due to the strong electron-withdrawing properties of the dicyanomethylene. Increasing the π-conjugation upon increasing the length of the thienylenevinylene in **1b** results in a wider absorbance.

In the solid state, the absorption maximum for **1a** is bathochromically shifted relative to those in solution, by 13 nm. **1b** shows a pronounced absorbance between of 400–850 nm, with a red-shifted maximum of 33 nm (764 nm). These results suggest that the extended backbone in **1b** results in stronger intermolecular π–π stacking interactions than in **1a** (Fig. 2). The estimated optical band gaps were calculated from the thin film absorbance onsets, and were 1.57 eV for **1a** and 1.50 eV for **1b**.

The fluorescence spectra display a red-shift of the emission band for compound **1b** in comparison to that for **1a**, around 30.2 nm, due

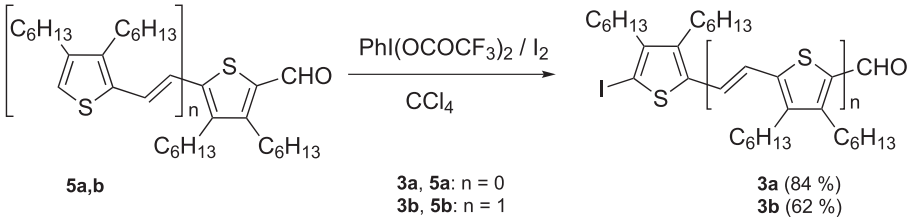

Scheme 2. Synthesis of precursor aldehydes **3a**, **b**.

Table 1
UV–Vis,[a] Fluorescence Emission[a] and OSWV[b] data for compounds **1a**, **b**.

	λ_{max} soln (nm)	log (ε)	λ_{max} film (nm)	λ_{em} (nm)	E^1_{ox}[b,c] (V)	E_{HOMO}[d] (eV)	E_{LUMO} (eV)	E_{0-0}[e] (eV)
1a	497	5.26	516	717	0.40	−5.50	−3.76	1.75
	705	5.04						
1b	542	5.17	734	747	0.26	−5.36	−3.67	1.69
	731	5.24						

[a] 10^{-5} M, in dichloromethane.
[b] 10^{-3} M in ODCB–acetonitrile (4:1) versus Fc/Fc^+ (E_{ox} = 0.04 V) glassy carbon, Pt counter electrode, 20 °C, 0.1 M Bu_4NClO_4, scan rate = 100 mV s^{-1}.
[c] Nonreversible processes.
[d] Calculated with respect to ferrocene, E_{HOMO}: −5.1 eV [40].
[e] Estimated from the intersection between the normalized absorption and normalized emission spectra at λ_{max}.

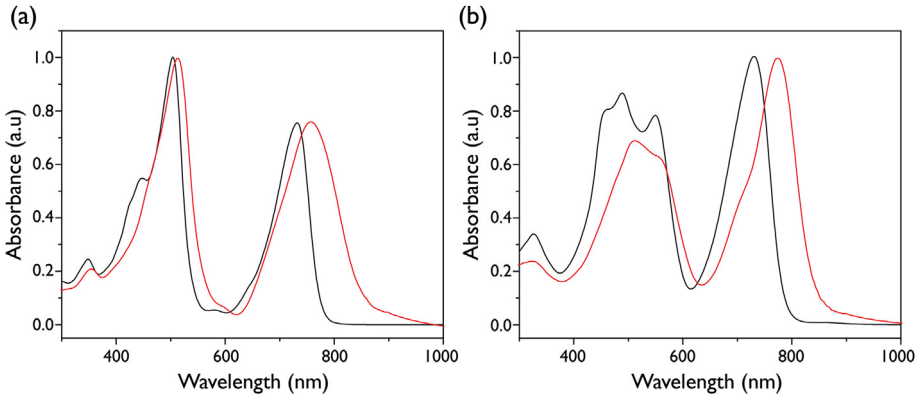

Fig. 2. Normalized UV–Vis spectra of **1a** (a) and **1b** (b) in DCM solution (black line) and in thin films (red line). (For interpretation of the references to color in this figure legend, the reader is referred to the web version of this article.)

to the increased conjugation by one more thienylenevinylene unit. If the emission spectra compounds **1a**, **b** are compared with those of the precursor aldehydes **4a**, **b** (Fig. S33), a significant quenching of the emission is observed, attributed to more efficient electron transfer processes.

3.3. Electrochemical properties

The electrochemical properties of **1a** and **1b** were investigated using Cyclic Voltammetry (CV) and Osteryoung Square Wave Voltammetry (OSWV) in *o*-DCB–acetonitrile (4:1) (Table 1, Fig. 3 and S34). In the anodic scan, both compounds show a first reversible one-electron oxidation wave at 0.40 V for **1a** (Fig. 4) and 0.26 V for

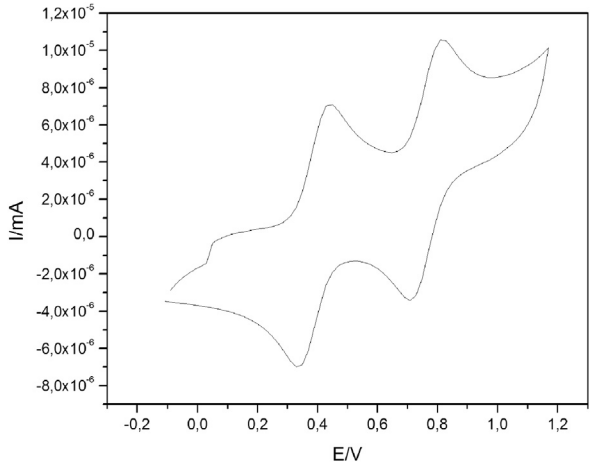

Fig. 3. CV plot of compound **1a**.

1b (vs Fc/Fc^+ in all cases) which correspond to the first oxidation of the porphyrin. For **1b**, the extended conjugation gives rise to a decrease of the E_{ox} value by 14 mV with respect to **1a**. A second reversible oxidation wave is observed at 0.78 V for **1a** and at 0.62 V for **1b**. Compound **1b** shows two more non-reversible oxidation waves at 0.93 and 1.02 V attributed to the oxidation of the thienylenevinylene moieties. The estimated E_{HOMO} values were calculated with respect to ferrocene as reference (E_{HOMO}: −5.1 eV) [40] and were determined to be −5.50 eV for **1a** and −5.36 eV for **1b**, in good agreement with the onset oxidation potentials.

Low-lying HOMO levels should result in high open-circuit voltages (V_{oc}) and are, therefore, desired [41–43]. The HOMO − LUMO gaps, optically determined, are as narrow as 1.75 and 1.69 eV for **1a** and **1b**, respectively. The E_{LUMO} of the dyes are higher than that E_{LUMO} of PCBM (−3.9 eV), with values of −3.75 and −3.67 eV for **1a** and **1b**, respectively. Hence, the LUMO energy levels of these small-molecules match quite well the LUMO energy of $PC_{61}BM$ (−3.9 eV) and $PC_{71}BM$ (−4.0 eV), which suggest an energetically favorable electron transfer from **1a** and **1b** to the acceptor moiety that should in turn favor the exciton dissociation.

3.4. Theoretical calculations

Theoretical calculations were carried out by density functional (DFT) at the B3LYP 6-31G* level *in vacuo* using Gaussian 03W to determine the more stable geometries for both dyes **1a** and **1b** (Fig. 4), the HOMO and LUMO energy levels and their molecular orbital contours.

The optimized structure of both **1a** and **1b**, show that the core is almost perfectly flat, with the aryl groups bounded to the porphyrin core being perpendicular to the macrocycle (dihedral angle of 90°), while the thienylenevinylene fragments are almost in the same plane with respect to the porphyrin rings with a dihedral angle

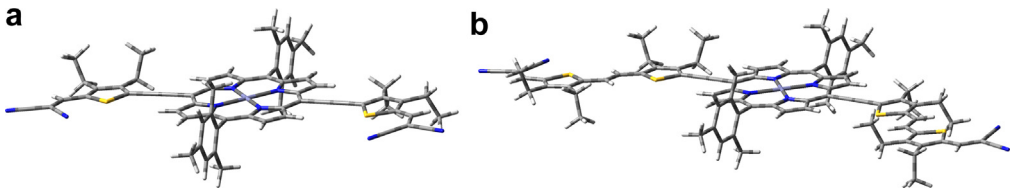

Fig. 4. Optimized geometries of dyes **1a** and **1b**.

around 0.5°. This planarity allows an extension of the conjugation between the porphyrin and the dicyanovinylene fragments. The bond lengths of the π-conjugated bridge between the porphyrin and the acceptor units are around 1.40 Å, both for single and double bonds, revealing a quinoid character. This fact suggests some zwitterionic contribution to the ground state.

The distribution of the orbital coefficients of the HOMO and LUMO states (Fig. 5) show that the charge density of the HOMO of **1a** and **1b** is delocalized over the whole conjugated system, the porphyrin and thienylenevinylene moieties. Similar to the HOMO, the LUMO spreads over the π-conjugated system. Since both orbitals, HOMO and LUMO (Fig. 5) are somewhat overlapped, this favors the HOMO to LUMO electronic transitions.

The theoretical HOMO − LUMO gaps are similar for both dyes, being slightly lower for compound **1b** (ΔE = 1.72 eV) than for **1a** (ΔE = 1.87 eV). This fact is mainly due to the more extended conjugation, increasing the HOMO level in **1b** and is related to the bathochromic shift of the maximum absorption wavelength of compound **1b** with respect to that for dye **1a** (according with the experimental data), which improves the light harvesting behavior. Finally, the offset between the LUMO of the donor (**1a** or **1b**) and the LUMO of the acceptor ($PC_{61}BM$ or $PC_{71}BM$) [41], from 0.54 eV to 1.01 eV, ensures efficient exciton dissociation at the D/A interface.

3.5. Photovoltaic properties

To explore the potential photovoltaic (PV) properties of **1a** and **1b**, solar cells were fabricated using the conventional sandwich structure of ITO/poly(3,4-ethylenedioxythiophene):polystyrenesulfonate (PEDOT:PSS)/small molecule: acceptor/Ca/Al. The active layer was spin-coated from chlorobenzene solutions. The ratio of **1a** and **1b** to $PC_{61}BM$ was adjusted, ranging from 1:1 to 1:4 (w/w), and the optimized value was found to be 1:2 for both of them. The optimized ratio was employed in a blend of **1a** and **1b** with $PC_{71}BM$. The photovoltaic devices were measured under an ambient atmosphere employing AM1.5G simulated illumination at an intensity of 100 mW/cm^2. The current density–voltage (J–V) characteristics and the external quantum efficiency (EQE) for the conventional device are shown in Fig. 6a–d and the performance parameters are summarized in Table 2 as a function of the weight ratios of Donor:$PC_{61}BM$.

Fig. 6b and d illustrates the best photovoltaic performances at varying D/A ratios. Photovoltaic devices containing **1a**:$PC_{61}BM$ exhibited high V_{oc} (0.86 V) at the optimized blend ratio of 1:2 w/w, with a short circuit current (J_{sc}) of 5.72 mA cm^{-2}, and a fill factor (FF) of 28.4% for an average PCE of 1.45%. Increasing as well as decreasing the amount of $PC_{61}BM$ resulted in a lower PCE. In contrast, photovoltaic devices incorporating a blend of **1b** and

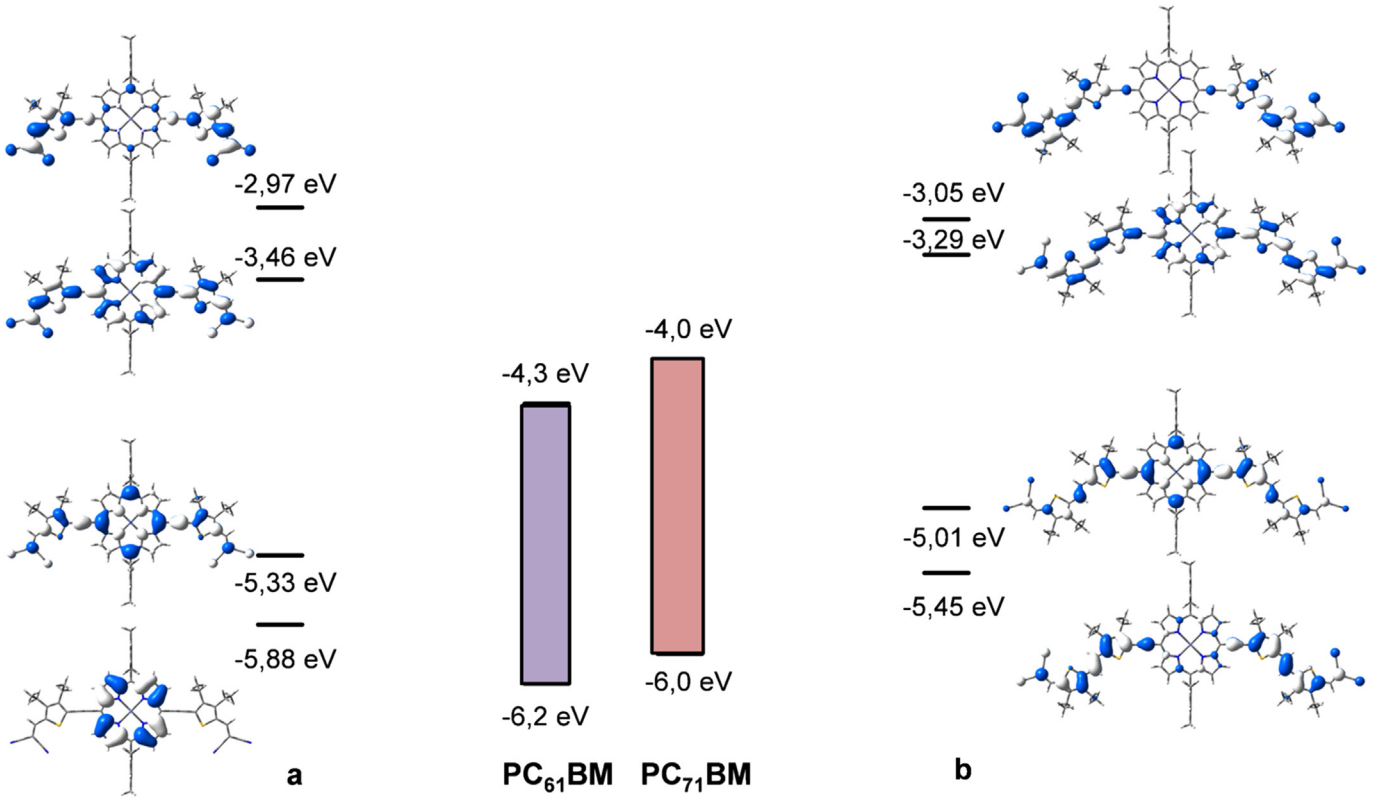

Fig. 5. Electronic density contours and energy levels for HOMO − 1, HOMO, LUMO, and LUMO + 1 calculated at the B3LYP/6-31G** level for dyes **1a** and **1b** compared with the energy levels of the $PC_{61}BM$ and $PC_{71}BM$ frontier orbitals.

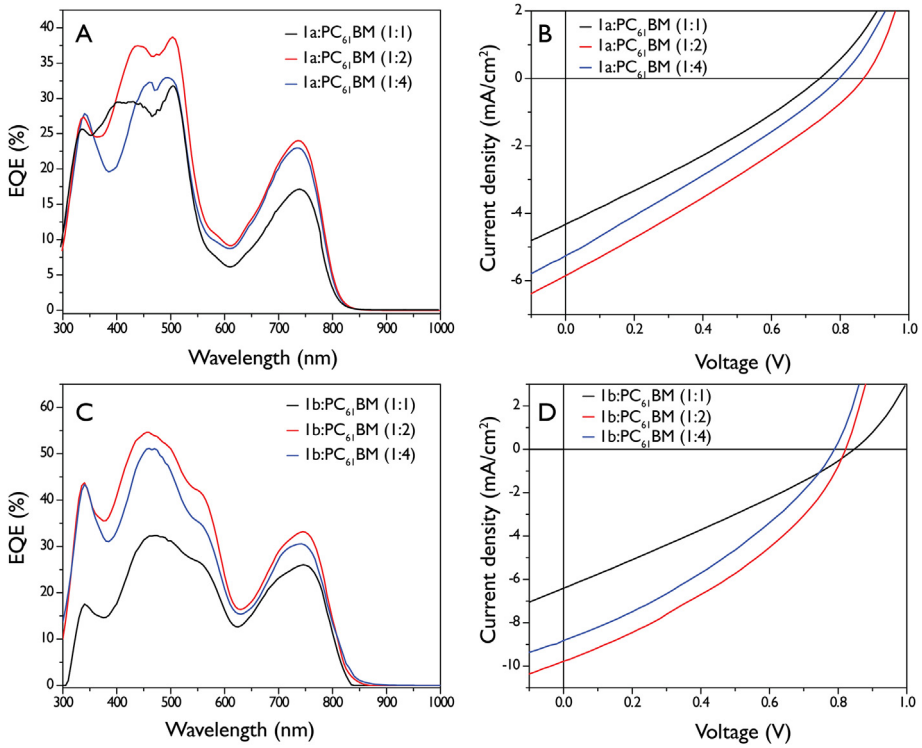

Fig. 6. EQE and *J*–*V* characteristics of the SMBHJ for **1a** and **1b** blending with $PC_{61}BM$ at different ratios.

Table 2
Summary of the photovoltaic performance of **1a** and **1b** blended with $PC_{61}BM$ and $PC_{71}BM$ under the illumination of AM1.5G, 100 mW/cm^2.

Active layer	V_{oc} (V)	J_{sc} (mA cm^{-2})	FF (%)	PCE [highest] (%)
1a:$PC_{61}BM$ (1:4)	0.78 ± 0.03	5.38 ± 0.33	27.8 ± 0.27	1.16 ± 0.1 [1.26]
1a:$PC_{61}BM$ (1:2)	0.86 ± 0.01	5.67 ± 0.12	28.1 ± 0.22	1.36 ± 0.1 [1.48]
1a:$PC_{61}BM$ (1:1)	0.63 ± 0.02	4.62 ± 0.13	29.1 ± 0.21	0.84 ± 0.1 [0.91]
1b:$PC_{61}BM$ (1:4)	0.79 ± 0.03	8.41 ± 0.21	33.2 ± 0.29	2.21 ± 0.1 [2.34]
1b:$PC_{61}BM$ (1:2)	0.82 ± 0.02	9.44 ± 0.26	35.0 ± 0.22	2.70 ± 0.1 [2.82]
1b:$PC_{61}BM$ (1:1)	0.84 ± 0.02	5.84 ± 0.30	27.3 ± 0.21	1.35 ± 0.1 [1.48]
1a:$PC_{71}BM$ (1:2)	0.84 ± 0.01	5.56 ± 0.12	26.4 ± 0.20	1.24 ± 0.1 [1.34]
1b:$PC_{71}BM$ (1:2)	0.82 ± 0.01	10.83 ± 0.24	35.7 ± 0.24	3.16 ± 0.1 [3.21]

$PC_{61}BM$ exhibited an average PCE of 2.70%, with a V_{oc} of 0.82 V, FF of 35.2% and a noteworthy J_{sc} of 9.79 mA cm^{-2}, because of its more efficient light absorbing properties. Average values were taken from 12 devices. The high values observed for the V_{oc} using **1a** are in agreement with the deeper HOMO level of **1a** (−5.50 eV) *vs* **1b** (−5.36 eV). The electron acceptor ($PC_{61}BM$) was replaced by $PC_{71}BM$ due to the broader absorbance and the higher extinction coefficient of the latter in the visible range. SMBHJ devices were fabricated with an architecture of ITO/PEDOT:PSS/**1b** or **1a**:$PC_{71}BM$ (1:2 w/w)/Ca/Al. Photovoltaic devices based on **1b** and $PC_{71}BM$ yielded an increased PCE of 3.21%, a remarkable 14% improvement, with an average J_{sc} of 10.83 mA cm^{-2}, V_{oc} of 0.82 V and a slightly

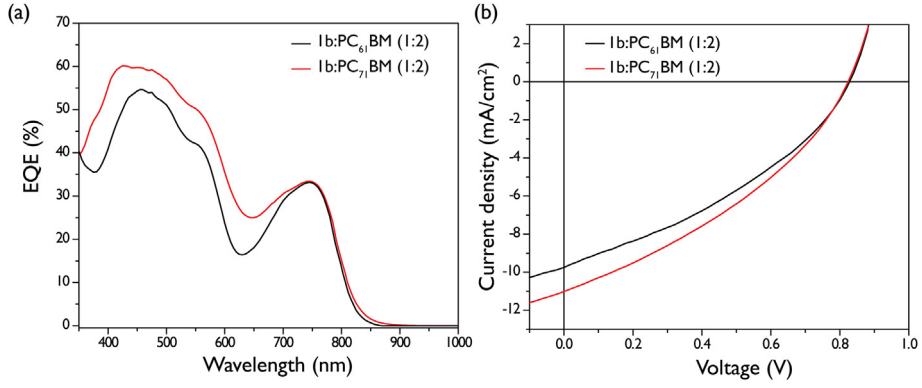

Fig. 7. EQE (a) and *J*–*V* (b) characteristics of the SMBHJ for **1b** blending with $PC_{61}BM$ and $PC_{71}BM$ in a 1:2 ratio.

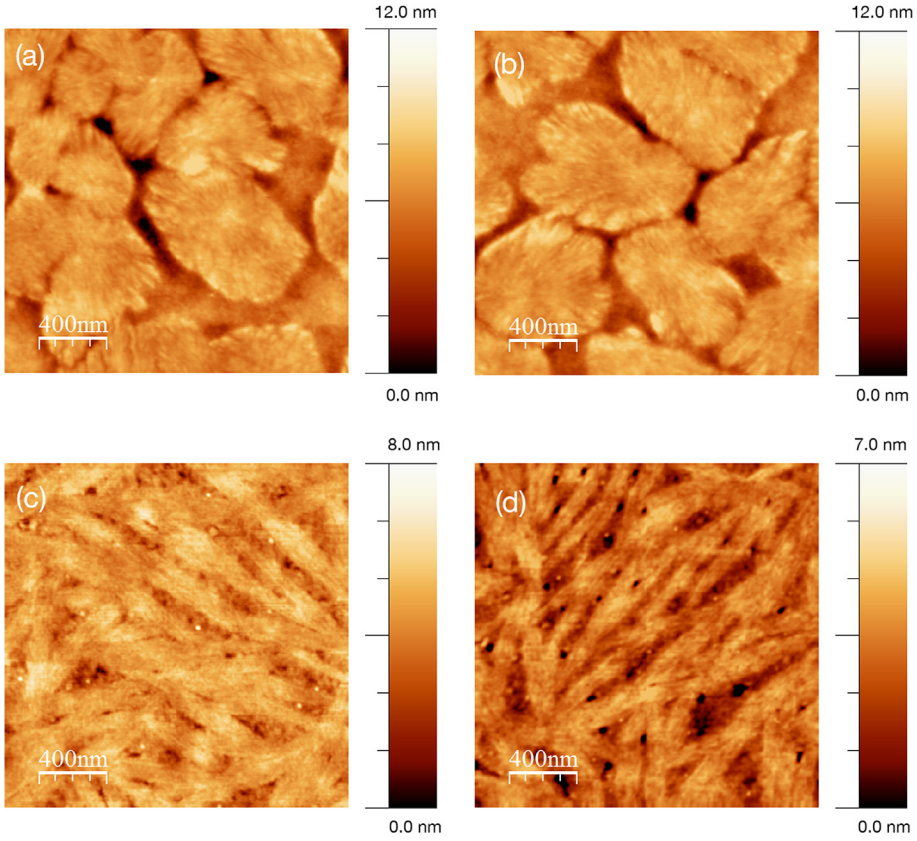

Fig. 8. Tapping mode AFM height images (2 μm × 2 μm) of **1a** films spin-coated from chlorobenzene blended with (a) $PC_{61}BM$ and (b) $PC_{71}BM$; tapping mode AFM height images (2 μm × 2 μm) of **1b** films spin-coated from chlorobenzene blended with (c) $PC_{61}BM$ and (d) $PC_{71}BM$.

improved FF (Fig. 7). Surprisingly, no improvement was observed employing **1a**:$PC_{71}BM$ (1:2 w/w) as the photoactive layer (see Fig. S36). In order to support the performances of the above devices, incident photo-to-current efficiency (IPCE) measurements were also conducted. As shown in Fig. 6b, the IPCE response of **1a** with $PC_{61}BM$ covers the visible spectrum ranging, from 300 nm to 800 nm, which matches the absorption spectra. The devices incorporating **1b** exhibited more efficient photoconversion efficiency than those based on **1a**, due to broader and higher IPCE response in the 300–600 nm range. Therefore, the addition of an extra unit of thienylenevinylene leads to a stronger light-harvesting small-molecule which results in a significant improvement in the power conversion efficiency. In addition, the IPCE values were further improved for a **1b**:$PC_{71}BM$ blend with a remarkable IPCE of 60% at 427 nm (Fig. 7). The theoretical J_{sc} values integrated from the EQEs are in good agreement with those experimentally observed in all cases (±5% mismatch).

Inspecting the morphology of the photoactive layers by atomic force microscopy using the tapping mode (AFM) provided some explanation for lower power conversion efficiencies obtained for the photovoltaic devices [44] incorporating **1a** and **1b** when blended with $PC_{61}BM$ and $PC_{71}BM$ (Fig. 8). The topography images for $PC_{61}BM$ and $PC_{71}BM$ reveal the formation of coarse morphologies with faceted islands features showing a root-mean-square roughness (rms) of 1.9 and 1.7 nm, respectively. Large aggregates of several hundred nanometers were observed which limit the exciton dissociation efficiencies and the charge transport, explaining the lower FF and J_{sc} values measured for these devices. On the other hand, the surface morphology of devices containing **1b**:$PC_{61}BM$ and **1b**:$PC_{71}BM$ exhibit a smoother surface topography (rms of 1.0 and 0.9 nm, respectively) with smaller aggregate sizes indicating better morphological features for exciton dissociation at the donor–acceptor interfaces, which correlate with the higher FF and J_{sc} and higher power conversion efficiencies observed.

4. Conclusions

In conclusion, we have synthesized two new conjugated acceptor–donor–acceptor (A–π-D–π–A) compounds having a Zn-porphyrin acting as donor and linked by ethynylenes to one or two units of thienylenevinylene and capped by dicyanovinylene groups as acceptor units. Incorporation of electron-accepting dicyanovinylene moieties through the thiophene based bridges shift the absorption profiles bathochromically to the NIR due to an intense intramolecular charge transfer band. **1a** and **1b** exhibit not only excellent light harvesting properties but also thermal stability and low-lying HOMO levels at −5.50 and −5.36 eV. Photovoltaic devices incorporating **1b** blended with $PC_{71}BM$ displayed a moderate PCE of 3.21% compared to that of **1a** (PCE of 1.4%). Extension of the conjugation in **1b** results in a significantly much higher J_{sc} and FF compared to that of **1a**. In order to chase higher efficiencies, further variations in the molecular structure are currently underway in our laboratories.

Acknowledgments

Financial support from the Ministry of Science and Innovation of Spain (CTQ2013-48252-P) and Junta de Comunidades de Castilla-La Mancha (PEII-2014-014-P) is gratefully acknowledged. SA thanks to the Fundación Carolina for a grant. LE wishes to thank the Robert A.

Welch Foundation for an endowed chair (AH-0033) and the National Science Foundation, grant DMR-1205302 (PREM Program) for generous financial support.

Appendix A. Supplementary data

Supplementary data related to this article can be found at http://dx.doi.org/10.1016/j.dyepig.2015.04.037.

References

[1] Yu G, Gao J, Hummelen JC, Wudl F, Heeger AJ. Science 1995;270:1789–91.
[2] Chen HY, Hou JH, Zhang SQ, Liang YY, Yang GW, Yang Y, et al. Nat Phot 2009;3:649–53.
[3] Li G, Zhu R, Yang Y. Nat Phot 2012;6:153–61.
[4] Yang T, Wang M, Duan C, Hu X, Huang L, Peng J, et al. Energy Environ Sci 2012;5:8208.
[5] Subbiah J, Purushothaman B, Chen M, Qin T, Gao M, Vak D, et al. Adv Mater 2015;27:702–5.
[6] Ameri T, Li N, Brabec CJ. Energy Environ Sci 2013;6:2390–413.
[7] Mishra A, Bäuerle P. Angew Chem Int Ed 2012;51:2020–67.
[8] Chen Y, Wan Y, Long G. Acc Chem Res 2013;46:2645–55.
[9] Heeger AJ. Adv Mater 2014;26:10–28.
[10] Roncali J, Leriche P, Blanchard P. Adv Mater 2014;26:3821–38.
[11] Kan B, Zhang Q, Li M, Wan X, Ni W, Long G, et al. J Am Chem Soc 2014;136:15529–32.
[12] Zhang Q, Kan B, Liu F, Long G, Wan X, Chen X, et al. Nat Phot 2015;9:35–41.
[13] Zhou J, Zuo Y, Wan X, Long G, Zhang Q, Ni W, et al. J Am Chem Soc 2013;135:8484–7.
[14] Sun Y, Welch GC, Leong WL, Takacs CJ, Bazan GC, Heeger AJ. Nat Mater 2012;11:44–8.
[15] Liu Y, Chen C, Hong Z, Gao J, Yang YM, Zhou H, et al. Sci Rep 2013;3:3356.
[16] Gust D, Moore TA, Moore AL. Acc Chem Res 2009;42:1809–18.
[17] Imahori H, Umeyama T, Ito S. Acc Chem Res 2001;34:40–8.
[18] Martínez-Díaz MV, de la Torre G, Torres T. Chem Commun 2010;46:7090–108.
[19] Li L-L, Diau EW. Chem Soc Rev 2013;42:291–304.
[20] Panda MK, Ladomenou K, Coutsolelos AG. Coord Chem Rev 2012;256:2601–27.
[21] Barea EM, Caballero R, López-Arroyo L, Guerrero A, de la Cruz P, Langa F, et al. ChemPhysChem 2011;12:961–5.
[22] Aljarilla A, Clifford JN, Pelleja L, Moncho A, Arrechea S, de la Cruz P, et al. J Mater Chem A 2013;1:13640–7.
[23] Mathew S, Yella A, Gao P, Humphry-Baker R, Curchod BFE, Ashari-Astani N, et al. Nat Chem 2014;6:242–7.
[24] Huang Y, Li L, Peng X, Peng J, Cao Y. J Mater Chem 2012;22:21841–4.
[25] Li L, Huang Y, Peng J, Cao Y, Peng X. J Mater Chem A 2013;1:2144–50.
[26] Qin H, Li L, Guo F, Su S, Peng J, Cao Y, et al. Energy Environ Sci 2014;7:1397–401.
[27] Sun Q, Dai L, Zhou X, Li L, Li Q. Appl Phys Lett 2007;91:253505/1–253505/3.
[28] Oku T, Noma T, Suzuki A, Kikuchi K, Kikuchi S. J Phys Chem Solids 2010;71:551–5.
[29] Hatano J, Obata N, Yamaguchi S, Yasuda T, Matsuo Y. J Mater Chem 2012;22:19258–63.
[30] Kumar CV, Cabau L, Koukaras EN, Sharma GD, Palomares E. Nanoscale 2015;7:179–89.
[31] Luechai A, Gasiorowski J, Petsom A, Neugebauer H, Sariciftci NS, Thamyongkit P. J Mater Chem 2012;22:23030–7.
[32] Kengthanomma T, Thamyongkit P, Gasiorowski J, Ramil AM, Sariciftcic NS. J Mater Chem A 2013;1:10524–31.
[33] Rawson J, Stuart AC, You W, Therien MJ. J Am Chem Soc 2014;136:17561–9.
[34] Chang CY, Cheng YJ, Hung SH, Wu JS, Kao WS, Lee CH, et al. Adv Mater 2012;24:549–53.
[35] Pellejà L, Dominguez R, Aljarilla A, Clifford JN, de la Cruz P, Langa F, et al. ChemElectroChem 2014;1(7):1126–9.
[36] Oswald F, Islam DMS, Araki Y, Troiani V, de la Cruz P, Moreno A, et al. Chem Eur J 2007;13:3924–33.
[37] Yu L, Muthukumaran K, Sazanovich IV, Kirmaier C, Hindin E, Diers JR, et al. Inorg Chem 2003;42:6629–47.
[38] Joydev KL, Dhanalekshmi S, Taniguchi M, Ambroise A, Lindsey JS. Org Proc Res Dev 2003;7:799–812.
[39] Jiang B, Yang SW, Barbini DC, Jones Jr WE. Chem Commun 1998:213–4.
[40] Cardona CM, Li W, Kaifer AE, Stockdale D, Bazan GC. Adv Mater 2011;23:2367–71.
[41] Cravino A. Appl Phys Lett 2007;91:243502.
[42] Dennler G, Scharber MC, Brabec CJ. Adv Mater 2009;21:1323–38.
[43] Scharber MC, Mühlbacher D, Koppe M, Denk P, Waldauf C, Heeger AJ, et al. Adv Mater 2006;18:789–94.
[44] Huang Y, Kramer EJ, Heeger AJ, Bazan GC. Chem Rev 2014;114:7006–43.